nature geoscience

Article

https://doi.org/10.1038/s41561-025-01681-9

Transient marine bottom water oxygenation on continental shelves by 2.65 billion years ago

Received: 1 March 2024

Accepted: 24 March 2025

Published online: 16 April 2025

Check for updates

Xinming Chen[1,2,3] ✉, Chadlin M. Ostrander[4], Brett J. Holdaway[3], Brian Kendall[5], Ariel D. Anbar[6,7], Sune G. Nielsen[8,9] & Jeremy D. Owens[3]

A growing body of evidence suggests that molecular oxygen (O_2) accumulated in some shallow marine environments beneath the effectively anoxic Archaean atmosphere 4.0 to 2.5 billion years (Ga) ago. Yet, the temporal and spatial distribution of these oxygen oases is not well known. Here we use thallium (Tl) isotope ratios, which are sensitive to manganese oxide burial, to place constraints on the timing and tempo of marine oxygen oases between about 2.65 Ga and 2.50 Ga. Lower-than-crustal authigenic $^{205}Tl/^{203}Tl$ ratios are common in shales from the approximately 2.65 Ga Jeerinah Formation (Western Australia) and the 2.50 Ga Klein Naute Formation (South Africa). Particularly low $^{205}Tl/^{203}Tl$ ratios are found at 2.50 Ga, coincident with a pronounced 'whiff' of O_2. These data can be explained by widespread seafloor manganese oxide burial, a scenario that requires persistent O_2 penetration into marine sediments beneath regionally extensive marine oxygen oases. By contrast, $^{205}Tl/^{203}Tl$ ratios from the 2.60–2.52 Ga Nauga Formation (South Africa) do not deviate from crustal values, suggesting an intervening period of muted seafloor Mn oxide burial. Our data suggest that O_2 accumulated over greater spatial extents and to greater depths than previously thought at about 2.65 Ga and that marine oxygenation was spatially and temporally dynamic well before the Great Oxidation Event began at about 2.4 Ga.

A variety of geochemical trends found in the Archaean sedimentary record at and after ~3.0 billion years (Ga) ago are very difficult to explain except as a consequence of the presence of O_2 (refs. 1–5). Morphologic evidence of cyanobacteria in fossilized stromatolites corroborate these geochemical data[6,7]. It appears that oxygenic photosynthesis evolved very early in Earth history, hundreds of millions of years before the initial rise of O_2 in Earth's atmosphere during the Great Oxidation Event (GOE)[8,9]. Yet, sulfur mass-independent fractionation (S-MIF) signatures that require a functionally anoxic atmosphere are found in sedimentary deposits throughout the Archaean[10]. To preserve S-MIF signatures in sedimentary minerals, the partial pressure of O_2 in Earth's Archaean atmosphere (pO_2) must have been less than 0.0001% the present atmospheric level according to the results of one-dimensional photochemical models[11,12].

Oxygen oases help to reconcile these seemingly incompatible Archaean data. It seems logical that rates of global O_2 production

[1]School of Oceanography, Shanghai Jiao Tong University, Shanghai, China. [2]Laboratory of Polar Ecosystem and Climate Change (Shanghai Jiao Tong University), Ministry of Education, Shanghai, China. [3]Department of Earth, Ocean, and Atmospheric Science, National High Magnetic Field Laboratory, Florida State University, Tallahassee, FL, USA. [4]Department of Geology and Geophysics, University of Utah, Salt Lake City, UT, USA. [5]Department of Earth and Environmental Sciences, University of Waterloo, Waterloo, Ontario, Canada. [6]School of Earth and Space Exploration, Arizona State University, Tempe, AZ, USA. [7]School of Molecular Sciences, Arizona State University, Tempe, AZ, USA. [8]Department of Geology and Geophysics, Woods Hole Oceanographic Institution, Woods Hole, MA, USA. [9]CRPG, CNRS, Université de Lorraine, Vandoeuvre lès Nancy, France. ✉e-mail: xchen6@sjtu.edu.cn

https://doi.org/10.1038/s41561-025-01681-9

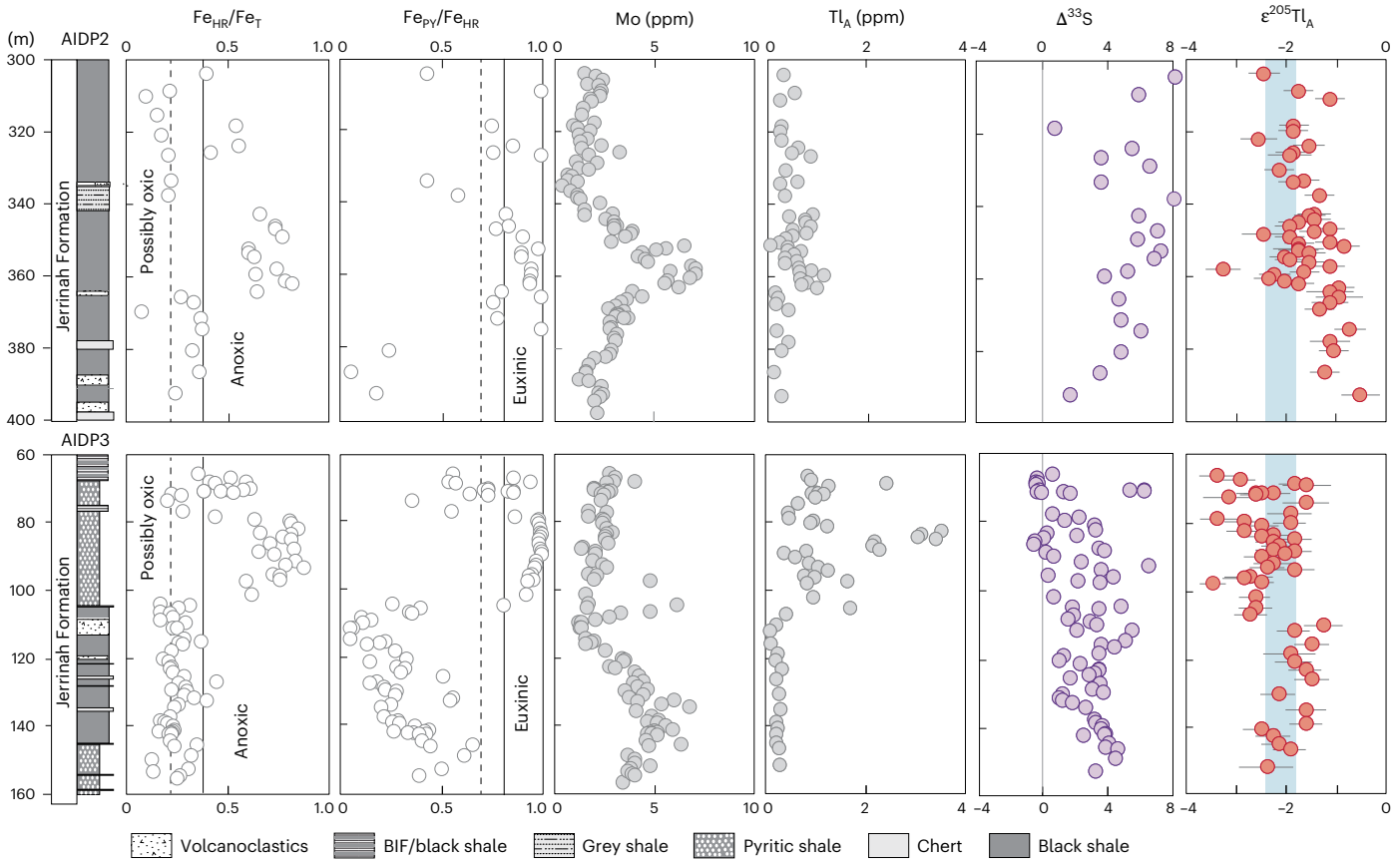

Fig. 1 | Geochemical profiles of the Jeerinah Formation in AIDP2 and AIDP3. Total Fe, highly reactive Fe and pyrite Fe are denoted by Fe_T, Fe_{HR} and Fe_{PY}, respectively. The solid black lines indicate the thresholds for local anoxia ($Fe_{HR}/Fe_T > 0.38$) or euxinia ($Fe_{PY}/Fe_{HR} > 0.8$); the dashed lines in Fe speciation panels represent relaxed thresholds for the same redox conditions ($Fe_{HR}/Fe_T > 0.22$ for anoxia and $Fe_{PY}/Fe_{HR} > 0.7$ for euxinia)[31]. Purple and red symbols are $\Delta^{33}S$ and authigenic Tl isotopic compositions ($\varepsilon^{205}Tl_A$), respectively. Stratigraphy, iron speciation, Mo concentration and $\Delta^{33}S$ data were from previous work[4,37,60]. The vertical blue bands represent the Tl isotopic composition of the bulk upper continental crust (BUCC, $\varepsilon^{205}Tl = -2.1 \pm 0.3$, 1 s.d., $N = 6$)[39]. All error bars represent two times the s.d. of that sample or the long-term external reproducibility of natural reference materials, whichever is larger. Thallium isotope data are presented as mean values ± 2 s.d. BIF, banded iron formation.

were low after photosynthesis initially evolved and, therefore, that the rate of O_2 production was outpaced by the rate of O_2 consumption by reductants exposed on, and delivered to, Earth's surface (for example, atmospheric methane, ultramafic/mafic rocks and volcanic gases)[13]. Nonetheless, localized O_2 accumulation in the vicinity of photosynthetic O_2 production—known as oxygen oases[14]—was possible without disturbing the global S-MIF signal[15,16]. These locations could have included biological soil crusts on land[17], lacustrine benthic mats[18], terrestrial mats[19] and productive shallow marine environments[20].

Many geochemical and morphological features of the Archaean sedimentary record can be linked to shallow marine oxygen oases[5,6,21–23], over variable extents and at various times beginning ~3.0 Ga ago[24]. Continuous long-term reconstructions of these environments, however, are elusive. Only a few continuous marine sedimentary deposits survive from the Archaean Eon, and the geochemical tools applied to them thus far to track oxygen oases generally struggle to constrain the extent and magnitude of oxygenation. The collective result of these shortcomings is a patchy record of marine oxygen oases, of uncertain extent.

The thallium isotope palaeoredox proxy

Thallium (Tl) isotopes can potentially see through these complications. Thallium isotopes are uniquely sensitive to seafloor Mn oxide burial[25,26]. Thallium isotope fractionation effects associated with removal to Mn oxide-rich sediments reach +12 to +18 ε-units[25]. Neither of the two other primary seawater Tl outputs drives a positive isotope fractionation effect; low-temperature basalt alteration results in a very minor negative effect (a few ε-units)[27], while sediments formed under anoxic conditions do not fractionate Tl isotopes whatsoever[28]. As Mn oxide burial requires the persistent penetration of O_2 below the sediment–water interface[29], the Tl isotope palaeoredox proxy is a unique tool capable of tracking O_2 accumulation specifically within marine sediment porewaters[23,26]. In doing so, Tl isotopes provide qualitative information about the intensity or magnitude of marine oxygenation.

More importantly, the isotopic cycling of Tl in the ocean is directly governed by global Mn oxide burial fluxes[28,30]. Therefore, Tl isotopes are a powerful tool to infer persistent O_2 penetration into marine sediments at a regional-to-global scale. This is in contrast to other proxies such as sedimentary iron speciation and redox-sensitive trace metal abundances and ratios that fingerprint the redox conditions only in the local water column[3,31].

Redox reconstruction with Tl isotopes is typically done by inferring past seawater Tl isotopic compositions ($\varepsilon^{205}Tl = (^{205/203}Tl_{sample}/^{205/203}Tl_{NIST\text{-}997} - 1) \times 10^4$) from measurements in ancient marine shales deposited under locally reducing conditions. Modern equivalent sediments are known to capture today's globally homogeneous seawater $\varepsilon^{205}Tl$ value, which is chiefly governed by the global extent of seafloor Mn oxide burial[28].

Thallium is rapidly removed from solution in sulfidic conditions, presumably in association with the formation of sulfide minerals (for example, pyrite)[28,32,33]. These sulfide minerals are thought to be the primary host phase of Tl in reducing sediments. Thallium removal either approaches quantitative extent or imparts negligible isotopic

fractionation in these settings because seawater $\varepsilon^{205}Tl$ values are observed in the sediments[33].

Of critical importance to this study, seawater $\varepsilon^{205}Tl$ capture by sedimentary sulfides is achieved over a wide range of depositional redox conditions today, essentially anywhere sedimentary Mn oxide minerals are unstable over long timescales. Sediments capture seawater $\varepsilon^{205}Tl$ values in all locations studied to this point where O_2 is absent from overlying bottom waters, and notably irrespective of bottom water H_2S contents (for example, the Black Sea, Baltic Sea, Cariaco Basin and Santa Barbara Basin)[28,34,35]. Seawater $\varepsilon^{205}Tl$ capture is even achieved in some sediments formed beneath O_2-bearing bottom waters, so long as O_2 does not persistently penetrate deep into sediment porewaters (for example, sediments from various productive upwelling zones)[36]. The fact that seawater $\varepsilon^{205}Tl$ capture occurs over such a wide range of depositional conditions today bodes well for reconstructions of past seawater $\varepsilon^{205}Tl$ values over large stratigraphic intervals of the ancient sedimentary record that, to be sure, were deposited under variable local redox conditions.

Late-Archaean shale sequences

Here, we apply Tl isotopes to some of the most well-preserved, well-studied and nearly continuous shale-dominated successions from the late Archaean. For all samples, we apply leaching protocols shown in previous work to effectively isolate 'authigenic' Tl associated with sedimentary sulfides[30]. It is these authigenic Tl isotope compositions ($\varepsilon^{205}Tl_A$) that are shown to capture seawater $\varepsilon^{205}Tl$ values[28,30].

The oldest targeted shales come from the ~2.65-Ga-old Jeerinah Formation from Western Australia preserved in drill cores AIDP2 and AIDP3. Both cores preserve continuous sequences of organic-rich shales deposited below wave base along a basinal depth gradient. Iron speciation and trace metal data from both cores suggest deposition under anoxic conditions conducive to seawater $\varepsilon^{205}Tl$ capture[37]. These data are plotted in Fig. 1. In brief, a high proportion of the total Fe (Fe_T) in shales from both cores resides in highly reactive Fe (Fe_{HR}) phases, which is, by analogy with modern sedimentary environments, suggestive of formation beneath anoxic bottom waters ($Fe_{HR}/Fe_T > 0.38$)[31]. Shales with lower Fe_{HR}/Fe_T ratios more consistent with locally oxic deposition ($Fe_{HR}/Fe_T < 0.22$) have generally higher Mo contents, suggesting that even these samples were probably formed under anoxic conditions[37]. A high proportion of pyritized Fe (Fe_{PY}) further suggests that shales from both cores were formed, at least at times, beneath anoxic and H_2S-bearing euxinic bottom waters ($Fe_{PY}/Fe_{HR} > 0.8$)[31].

We also target shales from the ~2.60- to ~2.50-Ga-old Nauga and Klein Naute formations from South Africa preserved in drill cores GKF01 and GKP01. These cores preserve continuous sequences of organic-rich shales deposited below wave base on the slope of a carbonate platform (GKF01) and the slope–basin transition (GKP01). Nauga Formation deposition occurred under mildly oxygenated bottom waters according to Fe speciation data and redox-sensitive trace element abundances (Fig. 2), with a high likelihood of shallow O_2 penetration into sediment porewaters based on high sedimentary Re/Mo ratios[3,38]. The younger Klein Naute Formation was deposited during broad marine transgression and, according to Fe speciation data, beneath anoxic (and at times euxinic) conditions more conducive to seawater $\varepsilon^{205}Tl$ capture[3].

Temporal evolution of late-Archaean oxygen oases

Lower-than-crustal $\varepsilon^{205}Tl_A$ values ($\varepsilon^{205}Tl_A < -2$) are common in the ~2.65-Ga-old Jeerinah Formation (Fig. 1) and ~2.50-Ga-old Klein Naute Formation (Fig. 2). In the Jeerinah Formation, the vast majority of low $\varepsilon^{205}Tl_A$ values are found in the AIDP3 drill core, reaching as low as -3.8 ± 0.3; 2 s.d. Low $\varepsilon^{205}Tl_A$ values are found in both cores that intersect the Klein Naute Formation, reaching as low as -4.2 ± 0.5; 2 s.d. in GKP01. These findings contrast with the Nauga Formation, where only one seemingly anomalous low $\varepsilon^{205}Tl_A$ value is found (Fig. 2); all other values from this unit are within error of the average bulk upper continental crust (-2.1 ± 0.3)[39].

The most straightforward and parsimonious interpretation of the lower-than-crustal $\varepsilon^{205}Tl_A$ values found in the Jeerinah and Klein Naute formations is that they track some extent of seafloor Mn oxide burial occurring elsewhere in the ocean at ~2.65 and ~2.50 Ga ago. The overwhelming majority of these low $\varepsilon^{205}Tl_A$ values come from sampling intervals of anoxic deposition preserved in AIDP3, GKF01 and GKP01. Low seawater $\varepsilon^{205}Tl$ values at ~2.65 Ga and ~2.50 Ga ago must have been at least regional in extent. By extension, the area of seafloor forming beneath O_2-bearing bottom waters with persistently oxygenated porewaters capable of Mn oxide burial must have also been at least regional in extent. If the residence time of Tl in late-Archaean seawater was longer than the ocean mixing time (cf. today), then this seawater $\varepsilon^{205}Tl$ value and the extent of seafloor Mn oxide burial required to promote it may have been globally representative. Unfortunately, we cannot differentiate between regional and global scenarios with the available data.

These inferences are corroborated by inorganic geochemical data reported in previous work. Multiple independent lines of evidence recovered from the AIDP2 and AIDP3 drill cores support mild O_2 accumulation during deposition of the Jeerinah Formation. These include, among other data, highly fractionated N isotopic ratios indicating an aerobic N cycle in shallow oxygenated waters and mild enrichments of redox-sensitive elements preferentially liberated during oxidative weathering of the continental crust[4]. Even stronger evidence is found for O_2 accumulation ~2.50 Ga ago in the Klein Naute Formation[3,40,41] and the broadly coeval Mt McRae Shale from Western Australia formed ~1,000 km away[1,21,42–44]. Of particular relevance to the present study, low $\varepsilon^{205}Tl_A$ values recovered from the upper member of the Mt McRae Shale point to regional (at least) bottom water O_2 accumulation on continental shelves ~2.50 Ga ago[23]. The Tl isotope data from the Klein Naute Formation corroborate the Mt McRae Shale findings, providing additional confirmation from a different region of at least regional water column oxygenation occurred. The Tl isotope data from the Jeerinah Formation extend evidence of regional marine O_2 accumulation specifically below the sediment–water interface backward by ~150 million years.

We are not aware of any viable alternative hypotheses that can explain the lower-than-crustal $\varepsilon^{205}Tl_A$ values. One possibility is preferential accumulation of the lighter-mass Tl isotope in sediments via biomass[33]. Biomass accumulation in sediments could potentially give rise to low sedimentary $\varepsilon^{205}Tl_A$ values. However, no low $\varepsilon^{205}Tl_A$ values convincingly linked to biomass have been found in modern organic-rich sediments formed below productive waters[33,36]. The lack of lower-than-crustal $\varepsilon^{205}Tl_A$ values in sediments from productive settings is probably due, at least in part, to the order-of-magnitude higher Tl abundances found in sedimentary sulfides (single $\mu g\ g^{-1}$)[28] relative to biomass (hundreds of $ng\ g^{-1}$)[45]. In other words, a substantial fraction of sedimentary Tl must originate from biomass to register a noticeable effect on sedimentary $\varepsilon^{205}Tl_A$ values. Again, we find lower-than-crustal $\varepsilon^{205}Tl_A$ values only in shales formed under sulfidic conditions shown today to strongly concentrate Tl in sediments, where it would seem especially unlikely to have a large fraction of the sedimentary Tl coming from biomass.

The most plausible location of bottom water O_2 accumulation in the otherwise anoxic Archaean oceans was beneath oxygen oases, probably in near-shore settings on and near the continental shelf. In these shallow-water locations, at water depths of many tens to potentially about a hundred metres[20], O_2 produced in the photic zone during oxygenic photosynthesis could persist at the sediment–water interface and penetrate into upper sediment porewaters. In marine environments today where bottom water O_2 accumulation is only transient (for example, seasonal), Mn oxides are not stable in sediments and are consumed

https://doi.org/10.1038/s41561-025-01681-9

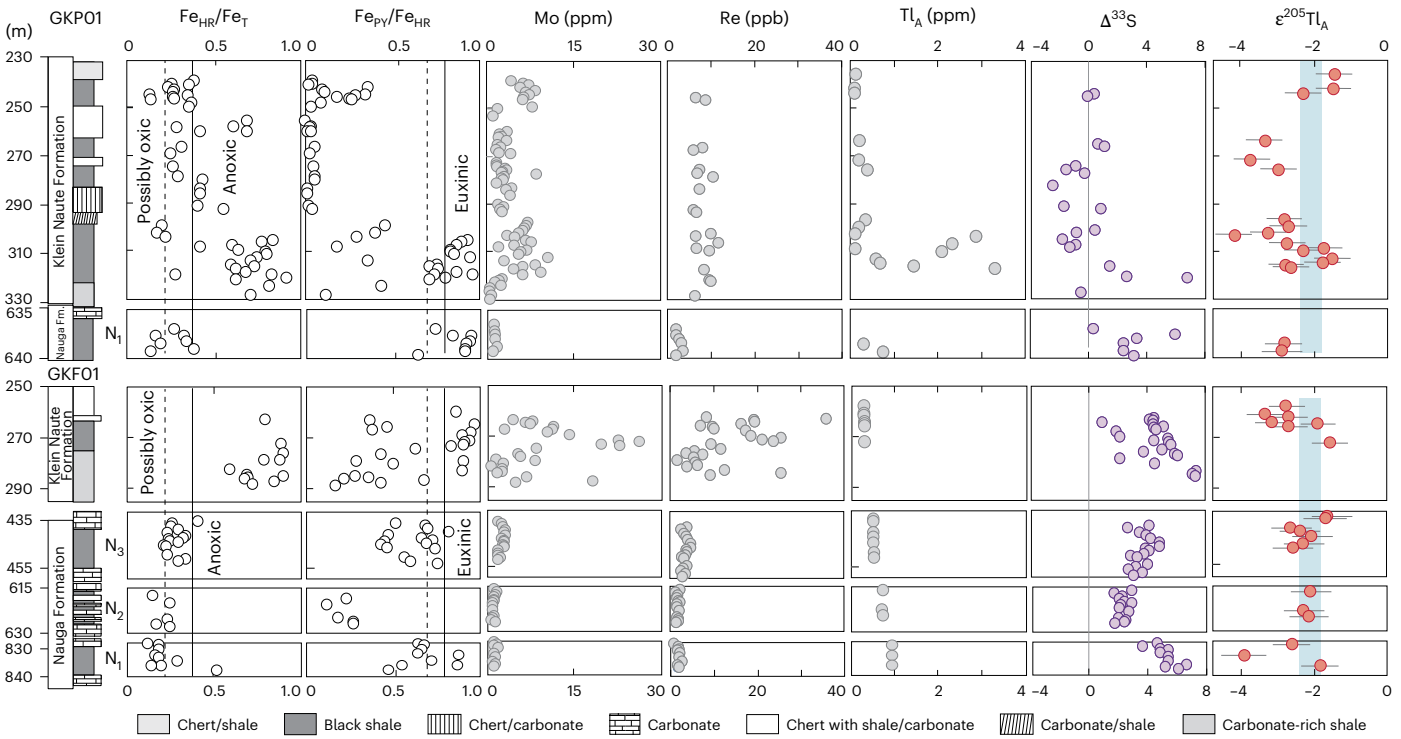

Fig. 2 | Geochemical profiles of the Klein Naute Formation and Nauga Formation in GKP01 and GKF01. Total Fe, highly reactive Fe and pyrite Fe are denoted by Fe_T, Fe_{HR} and Fe_{PY}, respectively. The solid black lines indicate the thresholds for local anoxia ($Fe_{HR}/Fe_T > 0.38$) or euxinia ($Fe_{PY}/Fe_{HR} > 0.8$); the dashed lines in Fe speciation panels represent relaxed thresholds for the same redox conditions ($Fe_{HR}/Fe_T > 0.22$ for anoxia and $Fe_{PY}/Fe_{HR} > 0.7$ for euxinia)[31]. Purple and red symbols are $\Delta^{33}S$ and authigenic Tl isotopic compositions ($\varepsilon^{205}Tl_A$), respectively. The vertical blue bands represent the Tl isotopic composition of the bulk upper continental crust (BUCC, $\varepsilon^{205}Tl = -2.1 \pm 0.3$, 1 s.d., $N = 6$)[39]. Stratigraphic, iron speciation, Mo and Re concentration and $\Delta^{33}S$ data were from previous work[3]. All error bars represent two times the s.d. of that sample or the long-term external reproducibility of natural reference materials, whichever is larger. Thallium isotope data are presented as mean values ± 2 s.d. Nauga N_1 = 637–641 m in GKP01, 829–839 m in GKF01; Nauga N_2 = 616–627 m in GKF01; Nauga N_3 = 440–455 m in GKF01.

during reductive dissolution[46,47]. Thallium is released during this dissolution process[32], precluding any net isotope fractionation[33]. Potential anaerobic Mn oxide formation pathways, such as photo-oxidation[48,49] and anoxygenic photosynthesis[50], are incompatible with the observed Tl isotope data because Mn oxides formed via either of these alternative pathways would be unlikely to survive transit through an underlying anoxic water column, let alone survive long-term burial in sediments with anoxic porewaters[51,52].

Shales from the Nauga Formation seem to have formed, at least at times, in a setting with oxygenated bottom waters. High Re/Mo ratios found in N2 and N3 shales[3] are reminiscent of those found in modern marine sediments where O_2 penetrates shallowly into sediment porewaters (<1 cm)[38]. Lower Re/Mo ratios and low authigenic Re and Mo enrichments in N1 shales, together with Fe speciation ratios consistent with locally oxic conditions, may indicate especially strong porewater O_2 penetration during early Nauga Formation deposition[3]. Sediments deposited today in various productive upwelling zones where O_2 penetrates shallowly into sediment porewaters can capture seawater $\varepsilon^{205}Tl$ values, but this capture is not guaranteed[36]. In contrast to the findings of ocean oxygenation at ~2.65 and ~2.50 Ga, near-crustal $\varepsilon^{205}Tl_A$ values recovered from shales deposited between ~2.60 Ga and ~2.50 Ga ago suggest limited seafloor Mn oxide burial through this time. Notably, persistently near-crustal $\varepsilon^{205}Tl_A$ values such as those found in a portion of the Nauga Formation are also found in coeval equivalents from Western Australia (the Wittenoom and Mt Sylvia formations)[53]. Together, and to first order, both sedimentary archives seem to suggest little to no regional seafloor Mn oxide burial between ~2.60 Ga and ~2.50 Ga ago and, hence, minimal penetration of O_2 into sediment porewaters at a regional scale.

It is difficult to identify the process(es) responsible for the higher-than-crustal $\varepsilon^{205}Tl_A$ values commonly found in the AIDP2 drill core. Elevated sedimentary $\varepsilon^{205}Tl_A$ values are found today almost exclusively in settings where Mn oxides are buried locally in sediments (ref. 36). However, AIDP2 shales would seem to preclude local Mn oxide burial due to locally anoxic depositional conditions. Oxide shuttling of isotopically heavy Tl to sediments from shallower oxygenated settings is a theoretical possibility but does not seem to impact sedimentary Tl isotope ratios in modern environments[26,34]. Note that we did not find a strong positive correlation between $\varepsilon^{205}Tl_A$ and Mn/Al ratios in AIDP2 (Supplementary Fig. 1). One observation that merits highlighting is that samples displaying the highest $\varepsilon^{205}Tl_A$ values in the proximal AIDP2 drill core have authigenic Tl abundances nearly an order-of-magnitude lower than those found in the more distal AIDP3 drill core (Fig. 1). Because of these considerably lower Tl concentrations, $\varepsilon^{205}Tl_A$ values in AIDP2 shales would potentially have been more prone to diagenetic (that is, secondary alteration), or to modification by local sources enriched in ^{205}Tl (for example, individual river or volcanic sources, which are sometimes enriched in ^{205}Tl today)[39,54].

Thallium isotope ratio data reported in this and previous studies from the two best-known windows into late-Archaean marine redox, compiled in Fig. 3, paint congruent pictures of a dynamic oxygen oases during the run-up to the GOE. Both archives suggest that O_2 accumulation in regional sediment porewaters below marine oxygen oases ~2.65 and ~2.50 Ga ago stimulated widespread Mn oxide burial on the late-Archaean seafloor. Importantly, these conditions were apparently transient, occurring over a period of a few million years according to temporal estimates for the ~2.50 Ga 'whiff' event[1,21]. The results of an isotope mass-balance model estimate a maximum fraction of total

https://doi.org/10.1038/s41561-025-01681-9

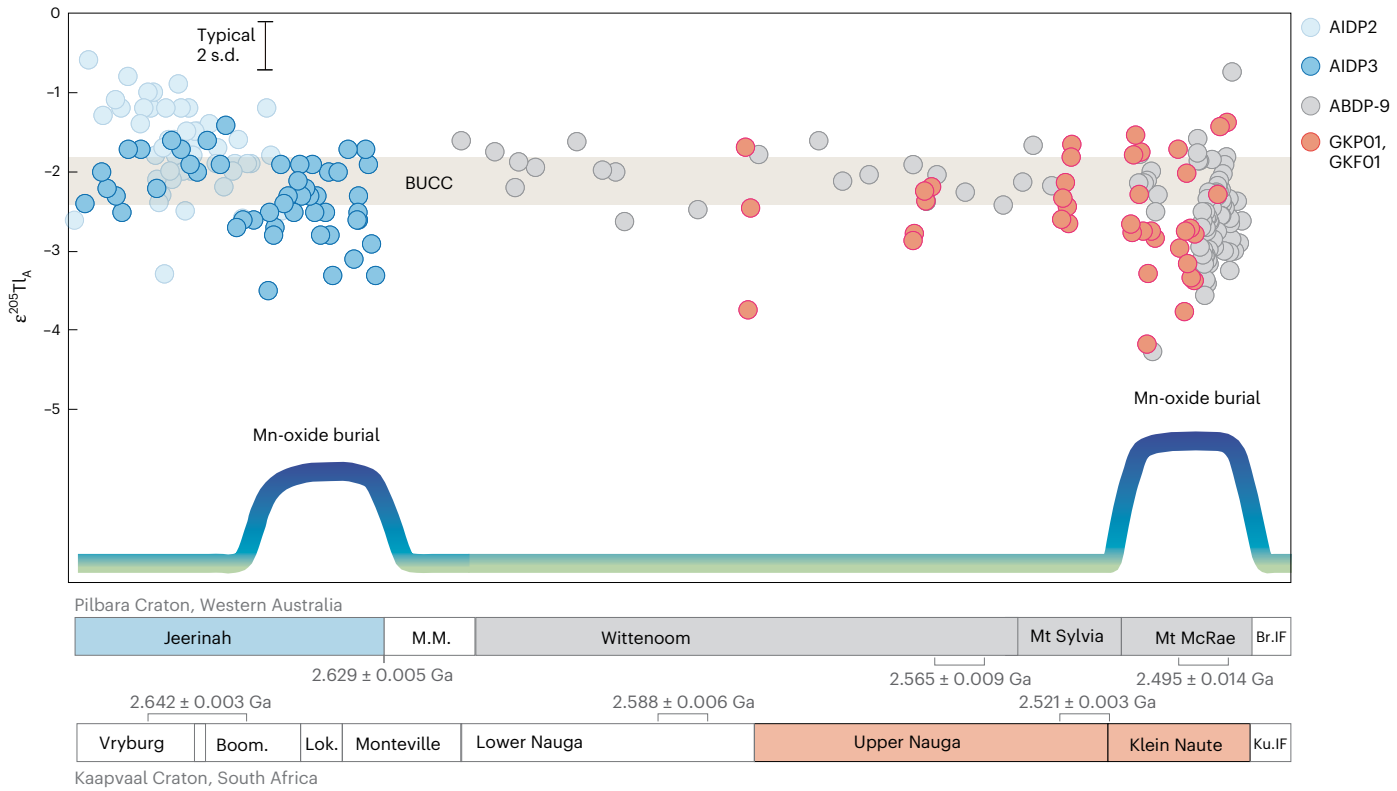

Fig. 3 | Summary of Tl isotope ratio data for the late-Archaean (~2.65 to 2.50 Ga) shales. The light-blue, blue, red and grey circles represent Tl isotope data from drill cores AIDP2, AIDP3, GKP01 + GKF01 and ABDP-9 (refs. 23,53), respectively. The horizontal band represents ε^{205}Tl of the bulk upper continental crust (BUCC, −2.1 ± 0.3; 1 s.d.; $N = 6$)[39]. The bold blue-green curve indicates the change of Mn oxide burial in the late-Archaean with two pulses of pronounced increases (two peaks in dark-blue colour) in Mn oxide burial at ~2.65 and 2.50 Ga. The blue, red and grey bars in the stratigraphic columns at the bottom correspond to shales from drill cores AIDP2 + AIDP3, GKP01 + GKF01 and ABDP-9. M.M., Marra Mamba; Br. IF, Brockman Iron Formation; Lok., Lokammona; Ku. IF, Kuruman Iron Formation; Boom, Boomplaas; Mt, Mount.

seawater Tl removal by Mn oxide-rich sediments of 10–19% and 14–23%, at ~2.65 Ga and ~2.50 Ga, respectively, which compare to the modern value of 40% (Methods and Supplementary Fig. 2). Shale Tl isotope data from the intervening timeframe between 2.60 Ga and 2.50 Ga support a much longer period of stunted seafloor Mn oxide burial separating these transient events, probably due to weakened or contracted marine oxygen oases. These data support emerging ideas of a dynamic initial Earth surface oxygenation[24,55–57]. But these oxygenation dynamics were apparently not limited just to the GOE, nor merely just to the atmosphere. These dynamics seem to predate the GOE, vary in magnitude and duration, and extend into the marine realm.

This work suggests that oxygen oases were spatiotemporally dynamic during the late Archaean. Why? Even today under a strongly oxygenated atmosphere that provides a steady supply of dissolved O_2 to the surface ocean, O_2 accumulation in shallow waters is spatially and temporally heterogeneous. Multiple factors are to blame: O_2 solubility negatively correlates with water temperature, leading to generally higher dissolved O_2 abundances in cold shallow waters at high latitudes; O_2 is not efficiently transferred between surface and deep waters where sharp temperature and salinity gradients hinder mixing, leading to generally lower dissolved O_2 abundances in shallow waters at low latitudes subjected to more heat and higher rates of evaporation; and high O_2 consumption rates in nutrient-rich upwelling areas can drive steep declines in dissolved O_2 abundances with depth, declines that are most pronounced during the especially productive summer months. In the absence of a near-infinite atmospheric O_2 source, surface ocean oxygenation during the late Archaean was probably even more heterogeneous[20]. Dissolved O_2 abundances in late-Archaean oxygen oases would have been subjected to the same physical forcings described above, but without possibility of rapid resupply from an effectively infinite atmospheric reservoir. Consider, for example, long-term temperature changes to Earth's surface over ten- to hundred-million-year timescales, which would have affected seawater O_2 solubility and water column mixing at individual localities. Or long-term changes in palaeocontinent configurations, ocean circulation patterns and nutrient availability, which would have affected O_2 production and consumption rates. The regional extent of shallow-ocean oxygenation at ~2.50 Ga, for example, was proposed to be associated with unusually stronger photosynthetic O_2 production due to enhanced nutrient supply from subaerial volcanism[58]. Transient O_2 accumulation events, that lasted for less than 10–100 million years, could have even surpassed the S-MIF threshold without effectively eradicating Earth's surface of S-MIF signals (the crustal memory effect[59]). If such strong O_2 accumulation did occur, it would have increased the potential for seafloor Mn oxide burial. Each of these effects would have manifested differently at different times and in different settings—in other words, in a spatially and temporally dynamic manner.

Online content

Any methods, additional references, Nature Portfolio reporting summaries, source data, extended data, supplementary information, acknowledgements, peer review information; details of author contributions and competing interests; and statements of data and code availability are available at https://doi.org/10.1038/s41561-025-01681-9.

References

1. Anbar, A. D. et al. A whiff of oxygen before the Great Oxidation Event? *Science* **317**, 1903–1906 (2007).

2. Crowe, S. A. et al. Atmospheric oxygenation three billion years ago. *Nature* **501**, 535–538 (2013).
3. Kendall, B. et al. Pervasive oxygenation along late Archaean ocean margins. *Nat. Geosci.* **3**, 647–652 (2010).
4. Koehler, M. C., Buick, R., Kipp, M. A., Stüeken, E. E. & Zaloumis, J. Transient surface ocean oxygenation recorded in the ~2.66-Ga Jeerinah Formation, Australia. *Proc. Natl Acad. Sci. USA* **115**, 7711–7716 (2018).
5. Planavsky, N. J. et al. Evidence for oxygenic photosynthesis half a billion years before the Great Oxidation Event. *Nat. Geosci.* **7**, 283–286 (2014).
6. Bosak, T., Liang, B., Sim, M. S. & Petroff, A. P. Morphological record of oxygenic photosynthesis in conical stromatolites. *Proc. Natl Acad. Sci. USA* **106**, 10939–10943 (2009).
7. Wilmeth, D. T. et al. Neoarchean (2.7 Ga) lacustrine stromatolite deposits in the Hartbeesfontein Basin, Ventersdorp Supergroup, South Africa: implications for oxygen oases. *Precambr. Res.* **320**, 291–302 (2019).
8. Fournier, G. P. et al. The Archean origin of oxygenic photosynthesis and extant cyanobacterial lineages. *Proc. R. Soc. B* **288**, 20210675 (2021).
9. Fischer, W. W., Hemp, J. & Johnson, J. E. Evolution of oxygenic photosynthesis. *Ann. Rev. Earth Planet. Sci.* **44**, 647–683 (2016).
10. Farquhar, J., Bao, H. & Thiemens, M. Atmospheric influence of Earth's earliest sulfur cycle. *Science* **289**, 756–758 (2000).
11. Catling, D. C. & Zahnle, K. J. The Archean atmosphere. *Sci. Adv.* **6**, eaax1420 (2020).
12. Pavlov, A. A. & Kasting, J. F. Mass-independent fractionation of sulfur isotopes in Archean sediments: strong evidence for an anoxic Archean atmosphere. *Astrobiology* **2**, 27–41 (2002).
13. Catling, D. C. in *Treatise on Geochemistry* 2nd edn (ed. Holland. H. D. & Turekian, K. K.) 177–195 (Elsevier, 2014).
14. Fischer, A. G. Fossils, early life, and atmospheric history. *Proc. Natl Acad. Sci. USA* **53**, 1205–1215 (1965).
15. Eickmann, B. et al. Isotopic evidence for oxygenated Mesoarchaean shallow oceans. *Nat. Geosci.* **11**, 133–138 (2018).
16. Fakhraee, M., Crowe, S. A. & Katsev, S. Sedimentary sulfur isotopes and Neoarchean ocean oxygenation. *Sci. Adv.* **4**, e1701835 (2018).
17. Lalonde, S. V. & Konhauser, K. O. Benthic perspective on Earth's oldest evidence for oxygenic photosynthesis. *Proc. Natl Acad. Sci. USA* **112**, 995–1000 (2015).
18. Sumner, D. Y., Hawes, I., Mackey, T. J., Jungblut, A. D. & Doran, P. T. Antarctic microbial mats: a modern analog for Archean lacustrine oxygen oases. *Geology* **43**, 887–890 (2015).
19. Finke, N. et al. Mesophilic microorganisms build terrestrial mats analogous to Precambrian microbial jungles. *Nat. Commun.* **10**, 4323 (2019).
20. Olson, S. L., Kump, L. R. & Kasting, J. F. Quantifying the areal extent and dissolved oxygen concentrations of Archean oxygen oases. *Chem. Geol.* **362**, 35–43 (2013).
21. Kendall, B., Brennecka, G. A., Weyer, S. & Anbar, A. D. Uranium isotope fractionation suggests oxidative uranium mobilization at 2.50 Ga. *Chem. Geol.* **362**, 105–114 (2013).
22. Riding, R., Fralick, P. & Liang, L. Identification of an Archean marine oxygen oasis. *Precambr. Res.* **251**, 232–237 (2014).
23. Ostrander, C. M. et al. Fully oxygenated water columns over continental shelves before the Great Oxidation Event. *Nat Geosci.* **12**, 186–191 (2019).
24. Ostrander, C. M., Johnson, A. C. & Anbar, A. D. Earth's first redox revolution. *Ann. Rev. Earth Planet. Sci.* **49**, 337–366 (2021).
25. Rehkämper, M. et al. Thallium isotope variations in seawater and hydrogenetic, diagenetic, and hydrothermal ferromanganese deposits. *Earth Planet. Sci. Lett.* **197**, 65–81 (2002).
26. Ostrander, C. M. et al. Thallium isotope cycling between waters, particles, and sediments across a redox gradient. *Geochim. Cosmochim. Acta* **348**, 397–409 (2023).
27. Nielsen, S. G. et al. Hydrothermal fluid fluxes calculated from the isotopic mass balance of thallium in the ocean crust. *Earth Planet. Sci. Lett.* **251**, 120–133 (2006).
28. Owens, J. D., Nielsen, S. G., Horner, T. J., Ostrander, C. M. & Peterson, L. C. Thallium-isotopic compositions of euxinic sediments as a proxy for global manganese-oxide burial. *Geochim. Cosmochim. Acta* **213**, 291–307 (2017).
29. Calvert, S. E. & Pedersen, T. F. Sedimentary geochemistry of manganese: implications for the environment of formation of manganiferous black shales. *Econ. Geol.* **91**, 36–47 (1996).
30. Nielsen, S. G. et al. Thallium isotopes in early diagenetic pyrite—a paleoredox proxy? *Geochim. Cosmochim. Acta* **75**, 6690–6704 (2011).
31. Raiswell, R. et al. The iron paleoredox proxies: a guide to the pitfalls, problems and proper practice. *Am. J. Sci.* **318**, 491–526 (2018).
32. Ahrens, J. et al. Thallium cycling in pore waters of intertidal beach sediments. *Geochim. Cosmochim. Acta* **306**, 321–339 (2021).
33. Ostrander, C. M. et al. Widespread seafloor anoxia during generation of the Ediacaran shuram carbon isotope excursion. *Geobiology* **21**, 556–570 (2023).
34. Chen, X. et al. Iron and manganese shuttle has no effect on sedimentary thallium and vanadium isotope signatures in Black Sea sediments. *Geochim. Cosmochim. Acta* **317**, 218–233 (2022).
35. Fan, H. et al. Constraining oceanic oxygenation during the Shuram excursion in South China using thallium isotopes. *Geobiology* **18**, 348–365 (2020).
36. Wang, Y., Lu, W., Costa, K. M. & Nielsen, S. G. Beyond anoxia: exploring sedimentary thallium isotopes in paleo-redox reconstructions from a new core top collection. *Geochim. Cosmochim. Acta* **333**, 347–361 (2022).
37. Olson, S. L. et al. Volcanically modulated pyrite burial and ocean–atmosphere oxidation. *Earth Planet. Sci. Lett.* **506**, 417–427 (2019).
38. Morford, J. L., Emerson, S. R., Breckel, E. J. & Kim, S. H. Diagenesis of oxyanions (V, U, Re, and Mo) in pore waters and sediments from a continental margin. *Geochim. Cosmochim. Acta* **69**, 5021–5032 (2005).
39. Nielsen, S. G. et al. Thallium isotopic composition of the upper continental crust and rivers—an investigation of the continental sources of dissolved marine thallium. *Geochim. Cosmochim. Acta* **19**, 2007–2019 (2005).
40. Ostrander, C. M. et al. An expanded shale δ^{98}Mo record permits recurrent shallow marine oxygenation during the Neoarchean. *Chem. Geol.* **532**, 119391 (2020).
41. Wille, M. et al. Evidence for a gradual rise of oxygen between 2.6 and 2.5 Ga from Mo isotopes and Re-PGE signatures in shales. *Geochim. Cosmochim. Acta* **71**, 2417–2435 (2007).
42. Stüeken, E. E., Buick, R. & Anbar, A. D. Selenium isotopes support free O_2 in the latest Archean. *Geology* **43**, 259–262 (2015).
43. Reinhard, C. T., Raiswell, R., Scott, C., Anbar, A. D. & Lyons, T. W. A late Archean sulfidic sea stimulated by early oxidative weathering of the continents. *Science* **326**, 713–716 (2009).
44. Garvin, J., Buick, R., Anbar, A. D., Arnold, G. L. & Kaufman, A. J. Isotopic evidence for an aerobic nitrogen cycle in the latest Archean. *Science* **323**, 1045–1048 (2009).
45. Flegal, A. R., Settle, D. M. & Patterson, C. C. Thallium in marine plankton. *Mar. Biol.* **90**, 501–503 (1986).
46. Froelich, P. N. et al. Early oxidation of organic matter in pelagic sediments of the eastern equatorial Atlantic: suboxic diagenesis. *Geochim. Cosmochim. Acta* **43**, 1075–1090 (1979).

47. Kristensen, E., Kristiansen, K. D. & Jensen, M. H. Temporal behavior of manganese and iron in a sandy coastal sediment exposed to water column anoxia. *Estuaries* **26**, 690–699 (2003).
48. Anbar, A. D. & Holland, H. D. The photochemistry of manganese and the origin of banded iron formations. *Geochim. Cosmochim. Acta* **56**, 2595–2603 (1992).
49. Liu, W. et al. Anoxic photogeochemical oxidation of manganese carbonate yields manganese oxide. *Proc. Natl Acad. Sci. USA* **117**, 22698–22704 (2020).
50. Daye, M. et al. Light-driven anaerobic microbial oxidation of manganese. *Nature* **576**, 311–314 (2019).
51. Lyons, T. W., Diamond, C. W. & Konhauser, K. O. Shedding light on manganese cycling in the early oceans. *Proc. Natl Acad. Sci. USA* **117**, 25,960–25,962 (2020).
52. Robbins, L. J. et al. Manganese oxides, Earth surface oxygenation, and the rise of oxygenic photosynthesis. *Earth Sci. Rev.* **239**, 104368 (2023).
53. Ostrander, C. M. et al. Shale heavy metal isotope records of low environmental O_2 between two Archean Oxidation Events. *Front. in Earth Sci.* **10**, 833609 (2022).
54. Baker, R. G. A., Rehkämper, M., Hinkley, T. K., Nielsen, S. G. & Toutain, J. P. Investigation of thallium fluxes from subaerial volcanism—implications for the present and past mass-balance of thallium in the oceans. *Geochim. Cosmochim. Acta* **73**, 6340–6359 (2009).
55. Lyons, T. W., Reinhard, C. T. & Planavsky, N. J. The rise of oxygen in Earth's early ocean and atmosphere. *Nature* **506**, 307–315 (2014).
56. Gumsley, A. P. et al. Timing and tempo of the Great Oxidation Event. *Proc. Natl Acad. Sci. USA* **114**, 1811–1816 (2017).
57. Poulton, S. W. et al. A 200-million-year delay in permanent atmospheric oxygenation. *Nature* **592**, 232–236 (2021).
58. Meixnerová, J. et al. Mercury abundance and isotopic composition indicate subaerial volcanism prior to the end-Archean "whiff" of oxygen. *Proc. Natl Acad. Sci. USA* **118**, e2107511118 (2021).
59. Reinhard, C. T., Planavsky, N. J. & Lyons, T. W. Long-term sedimentary recycling of rare sulphur isotope anomalies. *Nature* **497**, 100–103 (2013).
60. Zhelezinskaia I. *Sulfur Isotopic Records in Neoarchean Carbonates: Implications for the Early Precambrian Sulfur Cycle* (University of Maryland, 2018).

Methods

Sample digestion

Samples were digested following a procedure modified from previous literature[30]. About 100 mg of powdered samples were mixed with 3 ml of 2 M HNO_3 and heated at 130 °C for 12–15 h to extract the authigenic Tl from sedimentary sulfides. The soluble fraction was immediately digested at ~300 °C and 100 bars in a high-pressure asher for 1.5 h. After digestion, the samples were dissolved in 1 M HCl for anion-exchange chromatography.

Thallium purification

Thallium was purified using anion-exchange chromatography techniques described in previous literature[30,61]. Because of the relatively small sample sizes (~100 mg) used in this study, we used only one column to separate Tl from the matrix. This procedure was tested to be effective[62]. Approximately 8–20 h before Tl purification, ~100 µl of brominated water was added to each digested sample in 1 ml 1 M HCl. Approximately 100 µl of AG1X8 resin (200–400 mesh) were loaded to microcolumns. The resin was cleaned by passing 1.5 ml of 0.1 M HCl–SO_2 solution (5 wt.% SO_2). Then, the microcolumns were rinsed using 1.6 ml of 0.1 M HCl. Following this step, the resin was conditioned by 1 ml of 0.1 M HCl + 1% brominated water. After conditioning, samples dissolved in 1 M HCl + brominated water were loaded to the microcolumns. To remove the matrix, the resin was rinsed with 1.8 ml of 0.5 M HNO_3 + 3% brominated water, 1.6 ml of 2.0 M HNO_3 + 3% brominated water and 1.6 ml of 0.1 M HCl + 1% bromated water. Finally, Tl was eluted from the resin with 1.6 ml 0.1 M of HCl–SO_2 solution. The eluted solution was dried down completely at 180 °C to remove any residual sulfate and digested using ~100 µl aqua regia to remove any organic matter from the column chemistry. The samples were dissolved in 0.1 M HNO_3 + 0.1% H_2SO_4 for Tl isotope analysis. The yield of Tl during the purification process was ~100% within uncertainty. The amount of the procedural blank for Tl column chemistry was <5 pg, which was neglible compared with the amount of Tl (>10 ng) for our samples.

Thallium isotope analysis

Thallium isotopes were measured on a Thermo Scientific Neptune multicollector inductively coupled plasma mass spectrometer using an Aridus II desolvating nebulizer for sample introduction. Before isotope analysis, NIST SRM 981 Pb was added to every sample to monitor instrument mass bias. Thallium isotopes were analysed using the sample-standard bracketing method[63]. Thallium isotopic compositions are reported in ε notation relative to the reference standard NIST SRM 997 using

$$\epsilon^{205}\mathrm{Tl} = \left[\frac{\left(^{205}\mathrm{Tl}/^{203}\mathrm{Tl}\right)_{\mathrm{sample}}}{\left(^{205}\mathrm{Tl}/^{203}\mathrm{Tl}\right)_{\mathrm{NIST\ SRM997}}} - 1\right] \times 10{,}000. \quad (1)$$

The US Geological Survey shale reference material SCo-1 was processed and analysed with our samples to monitor accuracy. The measured authigenic ε^{205}Tl value (−2.8 ± 0.4; 2 s.d., N = 6) for SCo-1 was similar to previous studies (−2.9 ± 0.1, 3.0 ± 0.2 and −2.8 ± 0.3)[28,35,61–64]. The reported uncertainty of ε^{205}Tl for all our samples is either the 2 s.d. of SCo-1 (±0.3) or the measured samples, whichever is larger.

Mass-balance model for thallium isotopes

Under steady state, the mass balance of Tl isotopes in the oceans is described by

$$\epsilon^{205}\mathrm{Tl}_{\mathrm{IN}} = \epsilon^{205}\mathrm{Tl}_{\mathrm{OX}} \times f_{\mathrm{OX}} + \epsilon^{205}\mathrm{Tl}_{\mathrm{AOC}} \times f_{\mathrm{AOC}} + \epsilon^{205}\mathrm{Tl}_{\mathrm{ANO}} \times f_{\mathrm{ANO}}, \quad (2)$$

where $\varepsilon^{205}\mathrm{Tl}_i$ represents the isotopic composition of average inputs and the main marine outputs, f_i denotes the relative removal flux for each output, AOC and Tl-OX are low-temperature alteration of oceanic crust and well-oxygenated Mn oxide-rich sediments, and ANO stands for Tl removal by anoxic/euxinic sediments. Equation (2) can also be written as

$$\epsilon^{205}\mathrm{Tl}_{\mathrm{IN}} - \epsilon^{205}\mathrm{Tl}_{\mathrm{sw}} = \Delta^{205}\mathrm{Tl}_{\mathrm{OX}} \times f_{\mathrm{OX}} + \Delta^{205}\mathrm{Tl}_{\mathrm{AOC}} \times f_{\mathrm{AOC}} + \Delta^{205}\mathrm{Tl}_{\mathrm{ANO}} \times f_{\mathrm{ANO}}, \quad (3)$$

where $\Delta^{205}\mathrm{Tl}_{\mathrm{OX}}$, $\Delta^{205}\mathrm{Tl}_{\mathrm{AOC}}$ and $\Delta^{205}\mathrm{Tl}_{\mathrm{ANO}}$ (= 0) represent Tl isotopic offsets in oxic sediments, low-T alteration of oceanic crust and anoxic/euxinic Tl sinks relative to coeval seawater, respectively, and $\varepsilon^{205}\mathrm{Tl}_{\mathrm{sw}}$ is the Tl isotopic composition of seawater.

The manganese oxide sink causes the largest Tl isotope fractionation (13.5–19) with preferential uptake of heavier ^{205}Tl by the oxide[30]. Here, we use an isotope fractionation of 16 epsilon units for our Tl isotope mass balance[28]. Low-temperature alteration of oceanic crust imparts a much smaller fractionation (−2.5 to 0), but preferentially removes lighter Tl isotopes. If we use the smaller offset (that is, $\Delta^{205}\mathrm{Tl}_{\mathrm{AOC\text{-}sw}} = 0$), the estimated fraction of Tl removal by AOC would be magnified, making it implausible. Thus, we choose the offset of −1.14 epsilon units[28]. The Tl isotopic composition of the average inputs ($\varepsilon^{205}\mathrm{Tl}_{\mathrm{input}}$) into the oceans is about −1.8 (ref. 28).

We use a model with three sinks to generate a ternary plot of Tl isotopes (Supplementary Fig. 2), displaying the variations of seawater ε^{205}Tl due to changes in the relative fractions of Tl associated with AOC, oxic sediments and anoxic/euxinic sediments. The mass-balance model results reveal that Mn oxide-rich sediments are an important sink for Tl isotopes in the Neoarchaean oceans. The fractions of Tl associated with Mn oxide burial were estimated from the lightest $\varepsilon^{205}\mathrm{Tl}_{\mathrm{A}}$ at ~2.50 Ga and ~2.65 Ga (−4.3 ± 0.3 and −3.6 ± 0.3). The resulting maximum $f_{\mathrm{Tl\text{-}ox}}$ inferred from Tl isotope mass balance ranged between 10% and 19% and between 14% and 23% (Supplementary Fig. 2)[23], respectively, at ~2.65 Ga and ~2.50 Ga.

Data availability

All data related to this manuscript can be found in Supplementary Tables 1–3 and are also available via Figshare at https://doi.org/10.6084/m9.figshare.25212152 (ref. 65).

References

61. Nielsen, S. G., Rehkämper, M., Baker, J. & Halliday, A. N. The precise and accurate determination of thallium isotope compositions and concentrations for water samples by MC-ICPMS. *Chem. Geol.* **204**, 109–124 (2004).
62. Ostrander, C. M., Owens, J. D. & Nielsen, S. G. Constraining the rate of oceanic deoxygenation leading up to a Cretaceous Oceanic Anoxic Event (OAE-2: ~94 Ma). *Sci. Adv.* **3**, e1701020 (2017).
63. Nielsen, S. G., Rehkämper, M. & Prytulak, J. Investigation and application of thallium isotope fractionation. *Rev. Mineral. Geochem.* **82**, 759–798 (2017).
64. Bowman, C. N. et al. Linking the progressive expansion of reducing conditions to a stepwise mass extinction event in the late Silurian oceans. *Geology* **47**, 968–972 (2019).
65. Chen X. et al. Transient marine bottom water oxygenation on continental shelves by 2.65 billion years ago. *Figshare* https://doi.org/10.6084/m9.figshare.25212152 (2025).

Acknowledgements

G. White is thanked for instrumentation troubleshooting at the MagLab. This work was supported by National Aeronautics and Space Administration 80NSSC18K1532 (J.D.O.), 19-ICAR19_2-0007 (A.D.A.) and 80NSSC22K1628 (C.M.O. and S.G.N.) and the Sloan

Foundation FG-2020–13552 (J.D.O.), and a portion of this work was performed at the National High Magnetic Field Laboratory in Tallahassee, Florida, which is supported by the National Science Foundation Cooperative Agreement No. DMR-1644779 and by the State of Florida.

Author contributions

X.C. and J.D.O. developed the project idea. X.C. and B.J.H. processed samples and performed thallium isotope analyses with contributions from J.D.O. X.C., C.M.O. and J.D.O. wrote the paper with contributions from S.G.N., B.K. and A.D.A.

Competing interests

The authors declare no competing interests.

Additional information

Supplementary information The online version contains supplementary material available at https://doi.org/10.1038/s41561-025-01681-9.

Correspondence and requests for materials should be addressed to Xinming Chen.

Peer review information *Nature Geoscience* thanks James Kasting, Weiqiang Li and the other, anonymous, reviewer(s) for their contribution to the peer review of this work. Primary Handling Editor: Alison Hunt, in collaboration with the *Nature Geoscience* team.